ARTICLE IN PRESS

Environmental Research xxx (xxxx) xxx

Contents lists available at ScienceDirect

Environmental Research

journal homepage: www.elsevier.com/locate/envres

On the association between high outdoor thermo-hygrometric comfort index and severe ground-level ozone: A first investigation

Serena Falasca[a,b], Gabriele Curci[b,c], Ferdinando Salata[d,*]

[a] Department of Pure and Applied Sciences (DISPeA), University of Urbino, 61029, Urbino, Italy
[b] Center of Excellence in Telesensing of Environment and Model Prediction of Severe Events (CETEMPS), University of L'Aquila, 67100, L'Aquila, Italy
[c] Department of Physical and Chemical Sciences (DSFC), University of L'Aquila, 67100, L'Aquila, Italy
[d] Department of Astronautical, Electrical and Energy Engineering - Area Fisica Tecnica, University of Rome "Sapienza", Via Eudossiana 18, 00184, Rome, Italy

ARTICLE INFO

Keywords:
Air quality
Surface zone
Outdoor thermal comfort
Mediterranean outdoor comfort index
Weather research and forecasting model

ABSTRACT

According to the European Environment Agency, the year 2015 was the warmest on record to that point, with a series of heat waves from May to September resulted in high levels of tropospheric ozone. The implications of such a year on the human well-being and health are therefore of multiple nature and can be quantified referring to the exceedances of the corresponding thresholds. This work focused on the analysis of the May–September period of 2015 in the city of Milan (Italy) in terms of Mediterranean Outdoor Comfort Index (MOCI) and ozone concentrations, recorded by monitoring stations and modeled through the Weather Research and Forecasting model. Main findings show that thermo-hygrometric stress events (periods of at least six consecutive days characterized by daily maximum values of the MOCI higher than 0.5) are characterized by daily ozone higher than the guideline level of the World Health Organization (equal to 100 μgm^{-3}). This means that thermo-hygrometric stress conditions are added up to poor air quality conditions, with severe risks for human health. Moreover, a daily MOCI-daily ozone correlation coefficient equal to 0.6 was found for the whole period. The degree of correspondence between ozone events (defined according to the European Air Quality Directive) and MOCI events was also investigated pointing out that 86% and 95% of days during ozone events are correctly predicted by events of recorded and modeled MOCI respectively, with a corresponding false alarm rate of 3% and 9%.

1. Introduction

The Intergovernmental Panel on Climate Change (IPCC) recently estimated that a global warming approximately equal to 1.0 °C above pre-industrial levels have occurred and that such "global warming is likely to reach 1.5 °C between 2030 and 2052 if it continues to increase at the current rate" (IPCC, 2018).

The urban environment is particularly affected by such temperature increase, because of the urban heat island phenomenon (Falasca et al., 2016), with important consequences on the well-being and health of the inhabitants, from different points of view including thermo-hygrometric comfort and air quality (Salata et al., 2017a, 2017b).

Surface ozone is a pollutant included in the list of species affecting human health, vegetation and ecosystems (Block et al., 2012). It is a secondary species produced in the troposphere by oxidation of CO, methane, and non-methane volatile organic compounds (NMVOCs) by the hydroxyl radical (OH) in the presence of reactive nitrogen oxides (NOx) and sunlight (Jacob and Winner, 2009; Jenkin and Clemitshaw, 2002). Species such as CO, CH_4, NMVOCs and NOx are called "ozone precursors".

Ozone is dangerous for human health since it is a powerful oxidant that can react with a wide range of cellular components and biological materials. It may affect tissues of the respiratory tract or lung with symptoms such as cough, throat irritation, chest tightness, asthma attacks. In particular, it may cause asthma especially in children (Lee et al., 2004; Pollock et al., 2017; Wilhelm et al., 2009) or inflammation of the mucous membranes of the upper respiratory tract (Von Mutius, 2000). The higher sensitivity of some individuals to the effects of this species can be linked to genetic predisposition (Gilliland, 2009). Most of the evidence on effects of ozone in concentrations common in the troposphere relates to short term (hours) exposures (EEA, 2016; European Environmental Agency, 2019). Hence, it is crucial to control ozone formation to prevent negative effects on human health.

* Corresponding author.
E-mail address: ferdinando.salata@uniroma1.it (F. Salata).

https://doi.org/10.1016/j.envres.2020.110306
Received 4 June 2020; Received in revised form 2 September 2020; Accepted 1 October 2020
Available online 21 October 2020
0013-9351/© 2020 Elsevier Inc. All rights reserved.

Nomenclature

σ_c	standard deviation over the dataset
a	in the (2x2) contingency table, the number of hits
ARPA	Regional Environmental Protection Agency ("Agenzia Regionale per la Protezione Ambientale", in Italian)
b	in the (2x2) contingency table, the number of false alarms
BEP	Building Environment Parameterization
c	in the (2x2) contingency table, the number of misses
C_m	modeled values
C_o	observed values
d	in the (2x2) contingency table, the number of correct negatives
EEA	European Environment Agency
FAC2	Fraction of modeled values within a faction of two of observations
FR	False alarm Rate
GFS	Global Forecasting System
HR	Hit Rate
HW	Heat Wave
IPCC	Intergovernmental Panel on Climate Change
MB	Absolute Mean Bias
MOCI	Mediterranean Outdoor Comfort Index [-]
NCEP	National Center for Environmental Prediction
NMSE	Normalized Mean Square Error
NMVOCs	non-methane volatile organic compounds
O_3	surface or ground level ozone concentrations [μgm^{-3}]
O38h	8-h running mean [μgm^{-3}]
OMD	"Osservatorio Milano Duomo" (in Italian) foundation
PBLH	Planetary Boundary Layer Height [m]
R	correlation coefficient
RMSE	Root Mean Square Error
SOER	Report on the State of the Environment in Europe
WHO	World Health Organization
WRF	Weather Research and Forecasting model

According to the Report on the State of the Environment in Europe (Axiak and Sammut, 2002), 95% of the European urban population is exposed to concentrations of ozone above World Health Organization (World Health Organization, 2005) air quality guidelines, even if the reduction in emissions has led to a general improvement in air quality (European Environmental Agency, 2019; World Health Organization, 2005). Analysis of surface ozone trends carried out within the Tropospheric Ozone Assessment Report (Schultz et al., 2017) underlines that there is "less evidence for decreases of daytime average ozone at urban sites", compared to a decrease in ozone pollution in Europe (Chang et al., 2017).

Ozone pollution is critical usually in summer and for this reason the period from May through September is called the "ozone season". Due to the photochemical nature of the production processes, the connection between concentrations of surface ozone and meteorological variables (e.g. temperature, humidity, stability, wind speed, mixing depth) has been widely investigated (Otero et al., 2016; Porter et al., 2015; Porter and Heald, 2019). In particular, the key-role of the temperature on the ozone production is well recognized (Otero et al., 2016) and therefore still explored (Porter and Heald, 2019). In the context of a climate change with increasingly frequent and intense heat waves (HWs), recent studies focused also on the effect of HWs on ozone pollution both considering past HWs and climate change projections (Krug et al., 2019; Orru et al., 2019; Pyrgou et al., 2018). For example (Meehl et al., 2018), showed that surface ozone concentrations increase about 10%–60% on future HW days compared to non-HW days. Therefore, during high temperatures events, people are exposed to multiple risks, both thermal stress and ozone pollution. In this regard, Stowell et al., 2017 found out that under the Representative Concentration Pathways RCP8.5, increases in ozone concentrations are expected to product over 2200 additional premature deaths per annum in the US.

In order to limit human exposure to this pollutant and its impact on health, the European Directive 2008/50/EC on ambient air quality and cleaner air for Europe (implemented in Italy with the D.Lgs. 155/2010 (Presidente and Repubblica, 2010)) defines the following thresholds of ozone concentration for the protection of human health and vegetation: i) a long-term objective, expressed in terms of maximum daily 8-h mean and equal to 120 μgm^{-3}; ii) an information threshold, expressed in terms of hourly averaged value and equal to 180 μgm^{-3}; iii) an alert threshold, expressed in terms of hourly averaged value and equal to 240 μgm^{-3}.

As previously mentioned, another crucial aspect for the well-being of people especially in the frame of the climate change, is the thermo-hygrometric comfort. It is influenced by local microclimatic variables (e.g. temperature, wind speed, solar radiation, etc.) having a key-role also in the production of surface ozone. Temperature is the parameter most influencing outdoor comfort, but also the other microclimatic quantities play an important role. The outdoor thermo-hygrometric comfort can be quantified by means of suitable indexes, usually characteristic of specific geographical areas and populations. These indices are obtained on the basis of correlations between the values of measured meteorological quantities representative of the local microclimate and the thermo hygrometric sensations of a statistically valid sample of individuals making up the norm type of the population analyzed (Salata et al., 2016a).

Although extensive literature concerns ozone formation and outdoor thermo-hygrometric comfort, the question of possible relationships between these two parameters has not been addressed to the same extent.

The quality of urban outdoor spaces is considered a crucial goal for designers, engineers, urban planners, and lawmakers, etc. (Rosso et al., 2018). Therefore, a great effort is made all over the world to find solutions improving the quality of life in existing (even historical) neighborhoods and ensuring a high quality of life in neighborhoods to build, both from the point of view of thermal comfort and air quality (Deng and Wong, 2020; Rosso et al., 2018; Yuan et al., 2014). For example, (Krüger et al., 2011) observed and estimated relations between urban geometry and modifications in pedestrian thermal comfort and air quality within a city center in Brazil. (Falasca and Curci, 2018a) and (Falasca et al., 2019) studied the effect of mitigation strategies on air quality and also on outdoor comfort. However, a deep investigation on the environmental conditions determining a coexistence of poor outdoor air quality and thermo-hygrometric comfort is lacking in the scholarship. Therefore, this work is aimed at identifying and analyzing co-occurrences of thermo-hygrometric stress and heavy ozone events in the metropolitan area of Milan (Italy).

The period considered in this research runs from 1st May to 30th September, 2015. The choice of the year 2015 is due to the fact that it was characterized by the WHO as being a historically warm year globally. On average over Europe, 2015 was "the warmest year on record to that point" and the series of HWs affecting Europe from May to September 2015 resulted in high tropospheric ozone levels (European Environment Agency, 2017). During the year 2015, in Europe "41% of all stations reporting ozone with the minimum data coverage of 75% showed concentrations above the target value for the protection of human health", a considerably higher percentage than over the previous 5 years. Moreover, only 13% of all stations fulfilled the long-term objective, while 88% of the stations with exceedances of this value were background stations (European Environment Agency, 2017).

In the present work, the ozone season of year 2015 is characterized in

Table 1
Characteristics of the monitoring stations: species, network, name, geographical coordinates. For the air quality station, also the zone, the type and the international code are specified.

Species	Network	Name	Latitude	Longitude	Zone	Type	International Code
Weather	OMD ClimateNetwork®	Città Studi	45.479995	9.229652	–	–	–
Air quality	ARPA	Pascal Città Studi	45.4780	9.2360	Urban	Background	IT1692A

Fig. 1. The urban area of Milan (Italy). Red dots represent the monitoring stations, with the number 1 marking the weather station and the number 2 marking the air quality station. (For interpretation of the references to color in this figure legend, the reader is referred to the Web version of this article.)

terms of 8-h running averages (calculated from hourly recorded data, according to the European Directive, 2008/50/EC) and daily concentrations for surface ozone and in terms of hourly and daily values of Mediterranean Outdoor Comfort Index (MOCI), in order to find out potential coexistences of thermo-hygrometric stress and poor air quality circumstances. Thermo-hygrometric conditions consider other sides of the pedestrians' well-being in addition to the thermal side (indeed, the MOCI equation also contains wind speed, humidity and solar radiation). For this reason, the MOCI index is used for this analysis rather than only temperature.

2. Materials and methods

2.1. Characteristics of the study city

Milan is an important European economic, financial and cultural center. With about 1 million and 500 thousand inhabitants, it is the second most populous city in Italy (Municipality of Milan, 2020). It is located at the foot of Alps, in the center of the Po Valley, at about 120 m above the sea level.

The Po Valley is a geographical area of alluvial origin, unitary from the morphological and hydrographic points of view. Placed in southern Europe, it extends along northern Italy mainly within the water catchment area of the Po river, delimited by Alps to the North and West, the Northern Apennines to the South and the Upper Adriatic to the East. The Po Valley basin a humid temperate climate with very hot summer (Cfa, according to the Köppen-Geiger classification), when maximum temperatures can reach values higher than 38 °C. For example, the temperature reached 43 °C during the 2003 summer, under subtropical anticyclone conditions. Another characteristic of the Po climate is the lack of ventilation, which makes summer days even hotter and muggier, and generally amplifies the stagnation of pollutants, making the Po Valley one of the most polluted areas in Europe.

2.2. Observations

In this work, data from a weather station and an air quality station are used. Data of air temperature, wind speed intensity, relative humidity, solar radiation were acquired by the "Pascal Città Studi" weather station included in ClimateNetwork® of the Osservatorio Milano Duomo (OMD) foundation. Air temperature and wind intensity are used for the evaluation of the model performance, while all the weather variables are used for the computation of the MOCI. Data of ozone surface and NO_2 concentrations were downloaded from the website of the Regional Environmental Protection Agency (Italian acronym, ARPA) of the Lombardia region ("ARPA - Environmental issues/Air/Detection

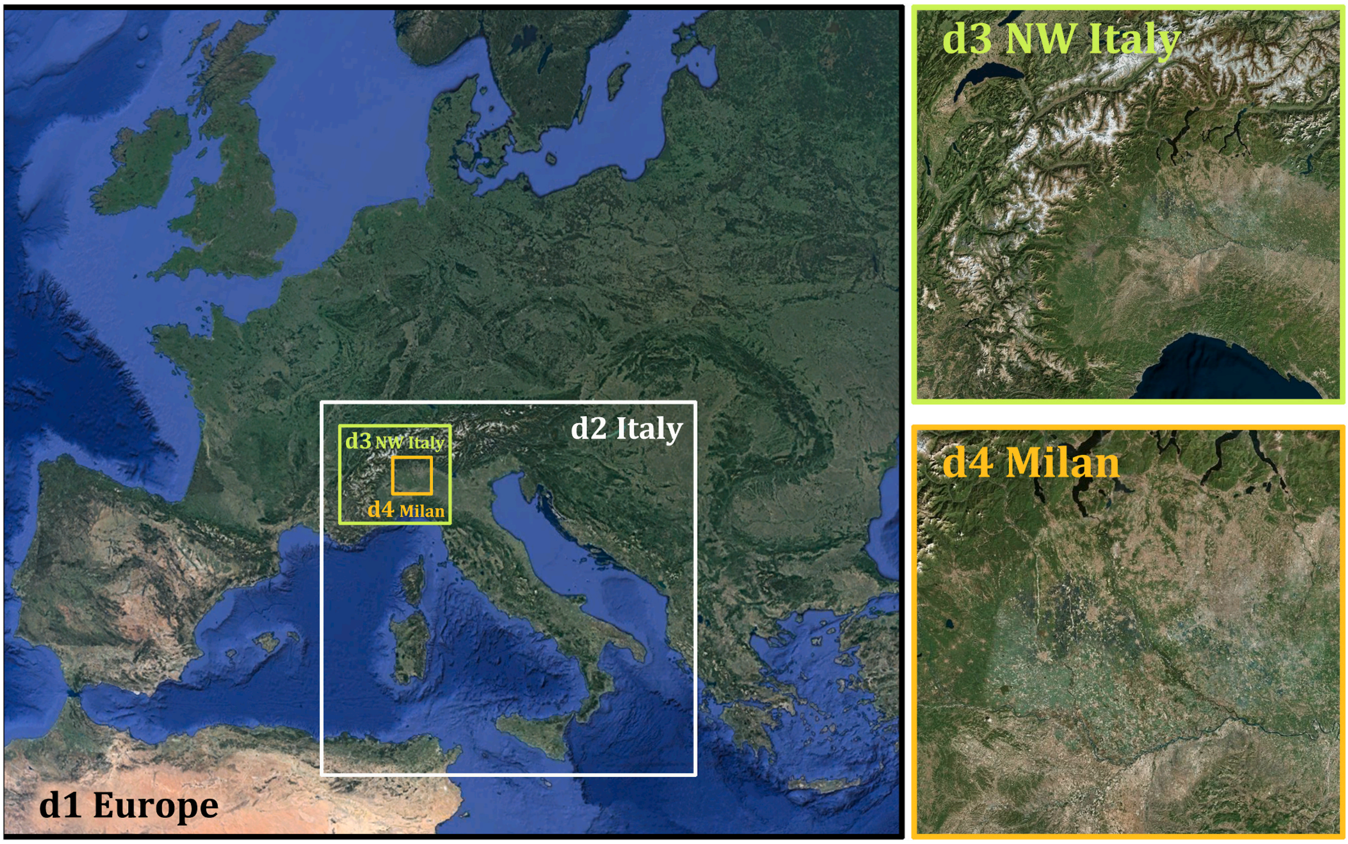

Fig. 2. Properties of the model domains: Geographical areas covered by the domains (Europe, Italy, North- Western Italy, urban area of Milan). Different colors correspond to different grid resolution. (For interpretation of the references to color in this figure legend, the reader is referred to the Web version of this article.)

network," 2020). The two selected stations are close, located in the same urban pattern and next to two parallel urban canyons. Their characteristics (species, name, geographical coordinates and zone, type and International code for air quality stations) are summarized in Table 1 and their geographical location is shown in Fig. 1.

2.3. The Mediterranean Outdoor Comfort Index

The MOCI equation, obtained through a transversal field survey in Rome by (Salata et al., 2016b) originally included the mean radiant temperature calculated using the globe temperature and the air temperature.

The MOCI is an index based on an ASHRAE (American Society of Heating, Refrigerating and Air-Conditioning Engineers) 7-point scale [-3; −2; −1; 0; +1; +2; +3], obtained thanks to a robust statistical survey. Such survey consisted in the compilation of a questionnaire involving a statistically valid cross sample and simultaneously the measurement of micro-meteorological quantities (air temperature, average radiant temperature, relative humidity, wind speed and global irradiation).

Subsequently, a relationship useful to predict (more precisely than other previous indices) the sensations of a norm type belonging to the Mediterranean population (i.e., habitually living in the Csa zone of the Köppen- Geiger climate classification (F. Salata et al., 2017a, 2017b; Salata et al., 2018a, 2018b)) was obtained through a Subsets Analysis.

Since the radiant temperature is not available in some applications, the Authors subsequently modified the equation in order to obtain a new version of the MOCI equation where the average radiant temperature is replaced by the total incident solar radiation. In this work, the following modified version of the MOCI equation is applied (Falasca et al., 2019):

$$MOCI = -4.257 + 0.325 \cdot I_{CL} + 0.146 \cdot T_A + 0.005 \cdot RH + 0.001 \cdot I_S - 0.235 \cdot WS \quad (1)$$

where I_{CL} is the thermal clothing insulation, T_A is the ambient temperature, RH is the relative humidity, I_S is the total incident radiation and WS is the wind speed intensity.

The thermal clothing insulation is a function of the ambient temperature (T_A) and is computed as:

$$I_{CL} = 1.608 - 0.038 \cdot T_A \quad (2)$$

Similarly to other indices, it is dimensionless and it is normally comprised in the range between −3 and +3. Values between −0.5 and + 0.5 correspond to thermo-hygrometric comfort conditions, while values lower than −0.5 and higher than +0.5 correspond to cold and hot conditions, respectively. In environments characterized by severe weather conditions, MOCI can be lower than such values and this means an important physical stress for people, due to extreme conditions compared to the needs of body thermoregulation. In this work, the threshold for well-being thermal condition is established at 0.5 (Golasi et al., 2016).

2.4. Ground-level ozone and standards

The second edition of the World Health Organization (WHO) Air quality guidelines for Europe established the guideline value for ozone at 120 μgm^{-3} for the 8-h daily average. However, according to the last version of the WHO Guidelines (dated back to 2005) new evidence from epidemiological studies reveal health effects at concentrations below the guideline level and positive associations between daily mortality and ozone levels. For these reasons, WHO reduced the guidelines level (for the daily maximum 8-h mean) from 120 μgm^{-3} to 100 μgm^{-3} (World

Table 2
Physics options used for simulations with the WRF model.

Category	Physics option
Microphysics	WSM6
Long wave radiation	RRTMG scheme
Short wave radiation	RRTMG scheme
Surface layer	Revised MM5 Monin-Obukhov
Land Surface	unified Noah land-surface model
Planetary Boundary Layer	Bougeault and Lacarrere
Urban Physics	Building Environment Parameterization (BEP)

Health Organization, 2005). However, in the European Directive on ambient air quality and cleaner air for Europe (2008/50/EC) (Parliament et al., 2008), implemented in Italy with the D.Lgs.155/2010 (Presidente and Repubblica, 2010), the long-term objective is fixed to 120 μgm^{-3}. In the same Directive, two other thresholds are specified, that is the information threshold and the alert threshold. Both are expressed in terms of hourly averaged value and are equal to 180 μgm^{-3} and 240 μgm^{-3}, respectively.

2.5. Model configuration

The Weather Research and Forecasting (WRF) model is used to reproduce the meteorological field in the urban area of Milan. The WRF model is a non-hydrostatic model, based on fully compressible Euler equations and described in detail in (Skamarock et al., 2008). It is widely used by research groups worldwide for meteorological and multidisciplinary applications. Here, the configuration tested in (Falasca and Curci, 2018b) and applied in (Falasca and Curci, 2018a), (Ciancio et al., 2018) and (Falasca et al., 2019) is adopted, with the only difference that two-way nesting is used instead of one-way nesting. The geographical areas covered by the four nested domains are visualized in Fig. 2, where different colors stand for different resolution of the horizontal grid. More in detail, domain 1 (framed in black in Fig. 2) covers Europe and is characterized by the coarsest horizontal resolution, equal to 36 km. Domain 2 (framed in white in Fig. 2) covers Italy and has a horizontal resolution of 12 km. Domain 3, covering the North-Western Italy with a horizontal resolution of 4 km, is framed in green in Fig. 2. Domain 4 (framed in orange in Fig. 2), centered over the urban area of Milan, presents the highest horizontal resolution, equal to 1.333 km. The vertical grid is common to the four domains and includes 33 eta vertical levels, with 11 levels in the first kilometer above the ground. The first level is at about 23 m and the top at 50 hPa. Initial and global boundary conditions are the Global Forecasting System (GFS) operational analyses of the National Center for Environmental Prediction (NCEP), with a spatial resolution of 1 ° × 1 ° and a temporal resolution of 6 h (National Centers for Environmental Prediction/National Weather Service/-NOAA/U.S, 2000). Land use information are provided by the MODIS

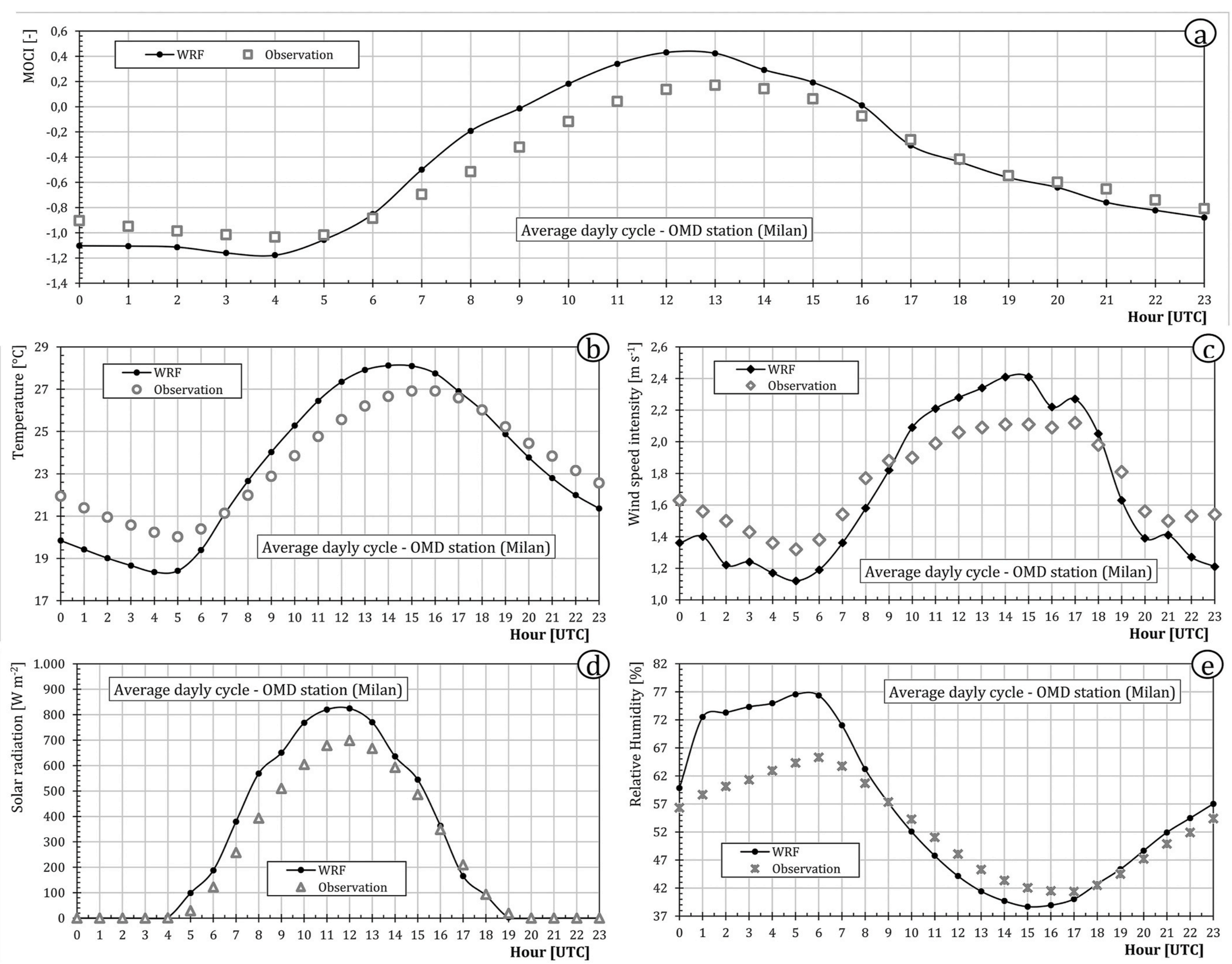

Fig. 3. Average daily trend of observed and model-simulated values in the period May–September of 2015: a) MOCI; b) air temperature; c) wind speed intensity; d) Solar radiation; e) Relative humidity.

dataset. In order to include the effects of urban surface heterogeneity and to reproduce the city-atmosphere exchanges within the urban canopy layer, a multi-layer urban canopy model is used, that is the Building Environment Parameterization (Martilli et al., 2002). Other physics options characterizing the WRF configuration are listed in Table 2.

2.6. Model evaluation

Consistently with the common use, the evaluation of the WRF model performance was carried out by comparing the hourly temperature and wind speed simulated by the WRF model with those acquired by the OMD weather station. The station considered does not provide any observations on the height of the planetary boundary layer (PBLH), therefore it is not possible to make a comparison of the simulated and observed values of this parameter. The following statistical parameters (Eqs. (3)–(8)) were computed to measure the reliability of the applied setup (Chang and Hanna, 2004):

– Absolute mean bias (*MB*):

$$\mathrm{MB} = \overline{\left|\mathrm{C_o} - \mathrm{C}_m\right|} \tag{3}$$

– fractional bias (FB):

$$FB = \frac{\left(\overline{C_o} - \overline{C_m}\right)}{0.5\left(\overline{C_o} + \overline{C_m}\right)} \tag{4}$$

– correlation coefficient (*R*):

$$R = \frac{\overline{\left(\mathrm{C_o} - \overline{\mathrm{C_o}}\right)\left(\mathrm{C}_m - \overline{\mathrm{C}_m}\right)}}{\sigma_{\mathrm{C_m}}\sigma_{\mathrm{C_o}}} \tag{5}$$

– normalized mean square error (NMSE):

$$NMSE = \frac{\overline{(C_o - C_m)^2}}{\overline{C_o}\,\overline{C_m}} \tag{6}$$

– root mean square error (RMSE):

$$RMSE = \sqrt{\overline{(C_o - C_m)^2}} \tag{7}$$

– fraction of modeled values within a faction of two of observations (*FAC2*):

$$0.5 \leq \frac{\mathrm{C}_m}{\mathrm{C_o}} \leq 2.0 \tag{8a}$$

where:

– C_m represents modeled values;
– $\mathrm{C_o}$ represents observed values;
– overbar $\overline{\mathrm{C}}$ represents average over dataset;
– σ_{C} represents the standard deviation over the dataset.

3. Results

This section illustrates: i) hourly values of weather variables (air temperature, wind speed, relative humidity and solar radiation) acquired by the OMD station; ii) hourly values of MOCI computed using these weather variables; iii) hourly values of surface ozone and NO_2 concentrations acquired by the air quality station; iv) hourly values of the PBLH simulated through the WRF model.

Table 3
Mean statistical parameters for the evaluation of the WRF model at the OMD weather station.

	MOCI	Temperature	Wind Speed	Solar radiation	Relative Humidity
➢ Mean Absolute Bias (MB)	0.049	0.19	0.046	48.36	3.08
➢ Fractional Bias (FB)	−0.10	−0.00065	−0.027	0.18	0.057
➢ Correlation Coefficient (R)	0.98	0.90	0.45	0.93	0.72
➢ Normalized Mean Square Error (NMSE)	0.14	$6.4 \cdot 10^{-5}$	0.28	0.26	0.055
➢ Root Mean Square Error (RMSE)	0.18	2.4	0.92	132.15	12.77
➢ Fraction of predictions within a factor of two of observations (FAC2)	0.63	1	0.75	0.43	0.99

For MOCI and ozone, also daily values are illustrated and analyzed: the daily value for ozone is computed as the maximum daily value of the 8-h mean of the hourly concentrations, in accordance with the European Directive on ambient air quality (Parliament et al., 2008). The daily value for MOCI is defined as the maximum of the hourly values of each day.

The evaluation of the WRF model performance in simulating weather variables is also carried out.

3.1. Evaluation of model performance

Fig. 3 compares the average daily cycle of MOCI (Fig. 3a) and meteorological variables (temperature, wind speed, solar radiation and relative humidity) acquired in the 2015 ozone season (May–September) by the OMD weather station, with the modeled values of the same quantities. MOCI values have been computed using both the recorded and simulated values of the weather quantities and following equation (1). Values of mean statistical parameters (defined in Section 2.6) used for the evaluation of the model's performance throughout the entire ozone season are collected in Table 3.

A perfect model should have MB, FB, NMSE and RMSE equal to zero and R and FAC2 equal to one.

The comparison between the recorded MOCI and the simulated MOCI (Fug. 3a) shows an underestimation by WRF during the night and an overestimation during the daytime. As will be discussed in more detail later, such overestimation can have positive implications in some applications of the model. The overestimation of MOCI by WRF is mainly a consequence of the positive bias of the temperature (Fig. 3b) and of the wind speed (Fig. 3c), which are characterized by the highest multiplicative coefficients in equation (1). In particular, temperature is also included in the term of thermal clothing insulation in equation (1). Relative humidity and solar radiation have much lower coefficients (in equations (1), 0.005 and 0.001 respectively), so their bias do not significantly influence the MOCI bias.

Table 3 shows that the fractional bias is included in a range between the very low value of the temperature (−0.00065) and the high value of the solar radiation (0.10). The R coefficient is low for the wind speed (0.45) while it reaches values characteristic of a very strong linear relationship for MOCI, Solar Radiation and temperature.

The FAC parameter is maximum and equal to 1 and 0.99 for temperature and relative humidity, while it is quite low for solar radiation (0.43).

Overall, although Table 3 shows that some quantities are much harder to simulate, according to the criteria provided by (Hanna and

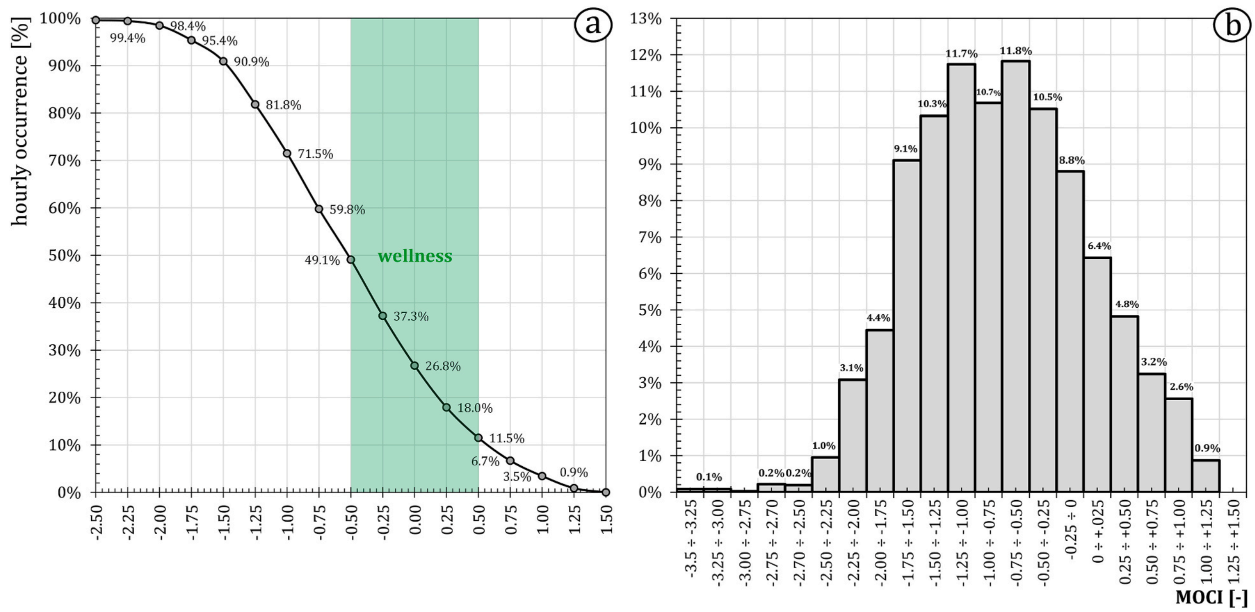

Fig. 4. Hourly MOCI values in the period May–September 2015: a) cumulative curve; b) percentage distribution. In (a) the green area represents the range of MOCI values characteristic of thermal well-being conditions. (For interpretation of the references to color in this figure legend, the reader is referred to the Web version of this article.)

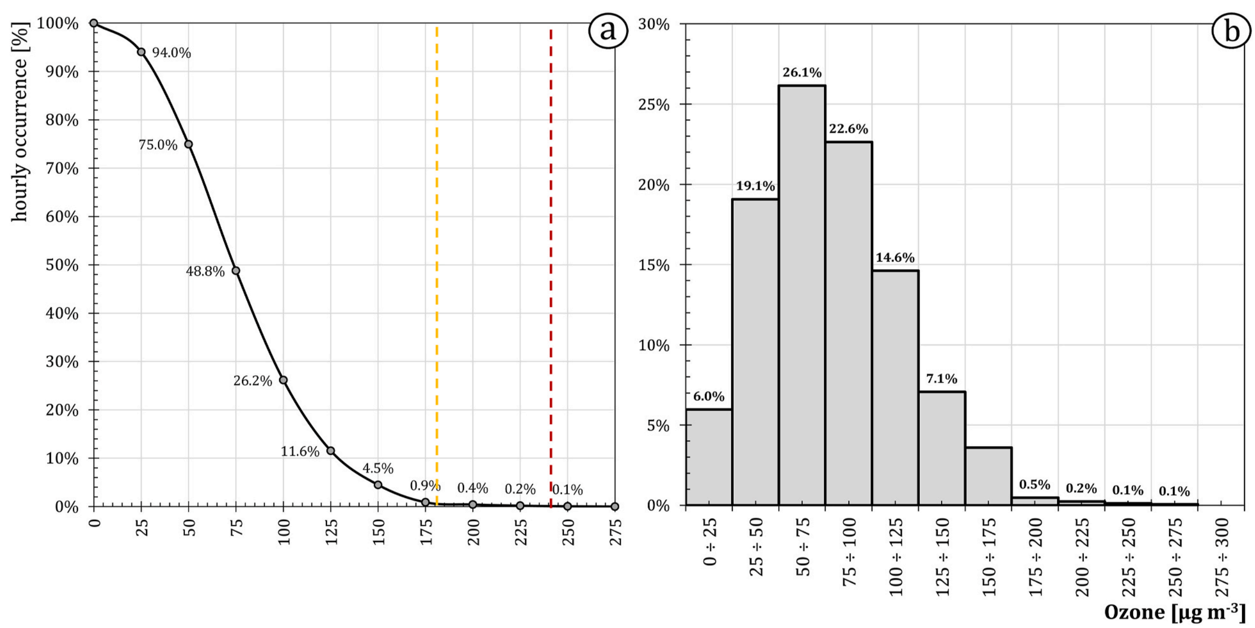

Fig. 5. Eight-hour running averages of hourly ozone concentrations in the period May–September 2015: a) cumulative curve; b) percentage distribution. In a) vertical lines represent the attention threshold (yellow dashed) and the alarm threshold (red dashed). (For interpretation of the references to color in this figure legend, the reader is referred to the Web version of this article.)

Chang, 2012) the tested WRF configuration is judged suitable for the simulations carried out in this work. In particular MOCI, that is the focus of this study, exhibits a good agreement between observed and modeled values.

With respect to the results of the work by (Falasca et al., 2019), where a 10-day period during July 2015 was simulated, the application of this modified setup (two-way nesting vs. one-way nesting) involves a decrease in the temperature nighttime bias from 4 °C to less than 2 °C, while the performance slightly worsen in the central hours of the day. As for the wind speed, an improvement in the model performance can be observed compared to previous applications over Milan (Falasca and Curci, 2018b).

3.2. *Characterization of the ozone season by means of hourly values*

This section includes hourly data of weather parameters and pollutants, both observed and simulated. In particular, the 8-h running averages are shown for the ozone, calculated from hourly data according to the European Directive 2008/50/EC.

Figs. 4 and 5 show the cumulative curve and the percentage distribution of hourly MOCI values and 8-h running averages of ozone concentrations in the period May–September 2015. The range of the MOCI

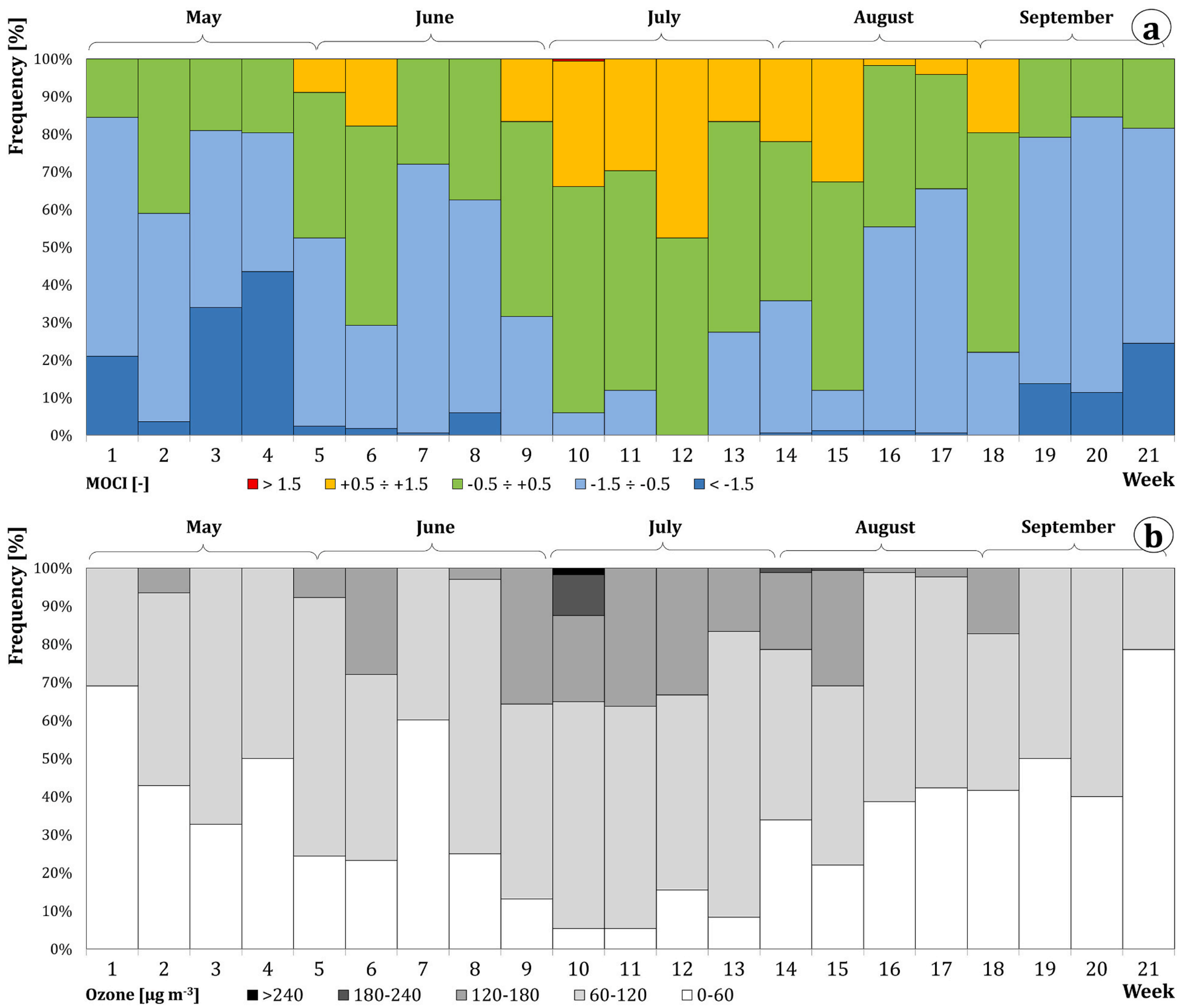

Fig. 6. Months of the 2015 ozone season; a) percentage distribution of the hourly values of MOCI; b) ozone.

values corresponding to thermal well-being conditions is emphasized thanks to the green area in Fig. 4a. And the values of attention and alarm thresholds defined in the European directive (Parliament et al., 2008) are visualized in Fig. 5a by means of the yellow and red vertical line, respectively.

Fig. 4a show that about the half of the total of hourly MOCI records is lower than thermal comfort conditions, while 7% is higher than thermal comfort conditions. Therefore, about 40% of total MOCI records are included in the thermal comfort range. Furthermore, the very low slope of the curve at the lower end of the range indicates that few records take on these values. For example, only 9% of records are less than −1.5. While the MOCI hourly records are mainly concentrated in the center of the observed range, the ozone records are concentrated towards the left part of the x axis.

Concerning hourly ozone records, the percentage of records above the European warning and alarm thresholds are very slight, less than 1%. The very high slope of the graph between 25 μgm^{-3} and 100 μgm^{-3} means that a large amount of data is concentrated in this range. In fact, these values correspond to percentage values equal to 96% and 26% in the cumulative curve (Fig. 5a) and also in the distributive curve (Fig. 5b) the bars included in this range are characterized by the highest percentages (up to 26%).

Fig. 6a and b shows the percentage distribution of the hourly values of MOCI and the 8-h running averages of ozone during the weeks of the 2015 ozone season. For both parameters, the range of observed values was divided into 5 ranges taking into account the thresholds used for the identification of outdoor thermal stress events and severe ozone events (described in sections 2.3 and 2.4, respectively). For MOCI only one threshold is defined (equal to 0.5), whereas for ozone three thresholds are defined in the European Directive: the long term objective (equal to 120 μgm^{-3}), the information threshold (equal to 180 μgm^{-3}) and the alert threshold (240 μgm^{-3}).

As for MOCI, the lowest values (less than −1.5) are present in some weeks during all the months of the ozone season 2015, except for the month of July. In June such values represent a percentage of a few percentage units, that is effectively negligible in the months of July and August. Values in the range between −1.5 and 0.5 are the most abundant and are present throughout the season. The MOCI assumes values between 0.5 and 1.5 only during June, July and August, with the highest percentages in July. Still in July, the only hourly value higher than 1.5 is observed. Basically, July is the month with the highest MOCI values.

Similar to MOCI, also for ozone July is characterized by the highest values. All the weeks of the 2015 ozone season are characterized by records in the range 0–60 μgm^{-3}, with percentages ranging from 70 to 80% in the first and last week of the period, to less than 10% in the central weeks of July. The 60–120 μgm^{-3} range is also widespread, with almost equal percentages throughout the period. The 120–180 μgm^{-3} range is mainly represented during the summer months (late June, July and early August) with percentages up to 35%. In May and September, most of records are under the threshold of 120 μgm^{-3} and in particular

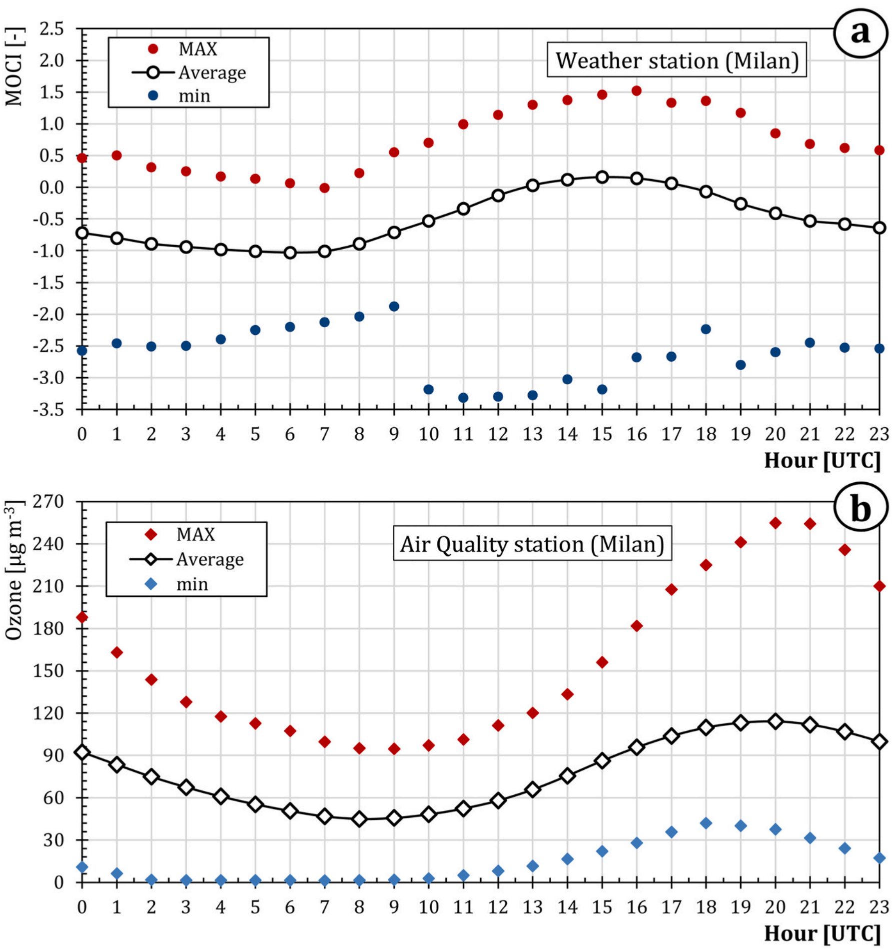

Fig. 7. Values of quantities in the ozone season 2015 (May–September): a) Maximum, average and minimum values of MOCI; b) Maximum, average and minimum values of the 8-h running averages of ozone concentrations. The red and blue markers respectively represent the maximum and minimum values for each hour of the day throughout the period. The black markers and line represent the daily cycle averaged over the same period. (For interpretation of the references to color in this figure legend, the reader is referred to the Web version of this article.)

more than 70% of records are lower than 60 μgm^{-3} in September.

More in detail, weeks number 5, 6, 9–18 present MOCI values linked to thermo hygrometric stress issues. In the same periods, there is a correspondence with the formation of high levels of ozone.

Fig. 7a and b shows the daily cycles of MOCI and O38h averaged over the period May–September 2015, together with maximum and minimum values for each hour of the day during the same period. The maximum and minimum values give the amplitude of the range in which the records of each quantity are included for each hour of the day. As regards the average daily cycle, that of the MOCI (Fig. 7a) has its minimum equal to about −1 at 6:00 a.m. and its maximum equal to about 0.2 at 3:00 p.m. The maximum values of the MOCI present a trend similar to the average daily cycle and are between 0 and 1.5. The minimum values, in contrast, have a trend greatly differing from the average daily cycle between 10:00 and 20:00 and have records between −3.5 and −1.9. The average daily cycle of O38h (Fig. 7b) has minimum and maximum values delayed with respect to MOCI: the minimum (equal to 45 μgm^{-3}) is at 8:00 a.m. and the maximum (equal to 115 μgm^{-3}) is at 20:00. The minimum values are between 1.3 μgm^{-3} and 42 μgm^{-3} and the maximum values are between 95 μgm^{-3} and 255 μgm^{-3}, with a trend similar to that of the average daily cycle.

In this section also the linear correlation between ozone and the following parameters is investigated: MOCI, weather quantities included in the computation of MOCI (i.e. temperature, wind speed, relative humidity, total radiation), PBLH and NO_2. To this end, Fig. 8 visualizes the scatter plot among each of the hourly quantities listed above.

Fig. 8 shows a positive and relatively high linear correlation ($r =$ 0,56) between MOCI and O38h. Among the parameters in the expression of the MOCI, a remarkable positive correlation can be observed between temperature and ozone ($r = 0.73$, higher than that of MOCI-ozone), a positive and much lower wind speed-ozone correlation ($r = 0.22$), a negligible radiation-ozone correlation ($r = 0.08$). A negative correlation is found between relative humidity and ozone ($r = -0.57$), and for both PBLH and NO_2-ozone correlations, which are very small and negative ($r = -0.21$ and $r = -0.29$, respectively). For these parameters, there is a decrease in ozone concentrations with increasing RH, PBLH and NO_2 concentrations. This picture is consistent with expected dependence of ozone on listed predictors (Porter et al., 2015; Porter and Heald, 2019). On the other hand, MOCI is highly correlated with temperature ($r =$ 0.94), and with solar radiation ($r = 0.61$) much more than ozone, and anti-correlated with RH ($r = -0.62$). This highlights the strong relationship among ozone, MOCI and temperature.

3.3. Characterization of the ozone season by means of daily maximum values

Since the thresholds for the identification of events characterized by outdoor thermal discomfort and high ozone concentrations are expressed in terms of maximum daily values, the characterization of the 2015 ozone season is carried out also in terms of daily maximum values of MOCI and ozone.

Similarly to Figs. 4 and 9 illustrates the percentage distribution of daily maximum values of MOCI and ozone in the five established ranges (see Section 3.2), both in the whole period May–September (Fig. 9a and c), than in the individual months (Fig. 9b and d).

Fig. 9a shows that most of the maximum daily MOCI values (98%) are between −1.5 and 1.5, with a prevalence of values between −0.5 and 0.5 (48%). Only 2% of the total is represented by daily values lower than

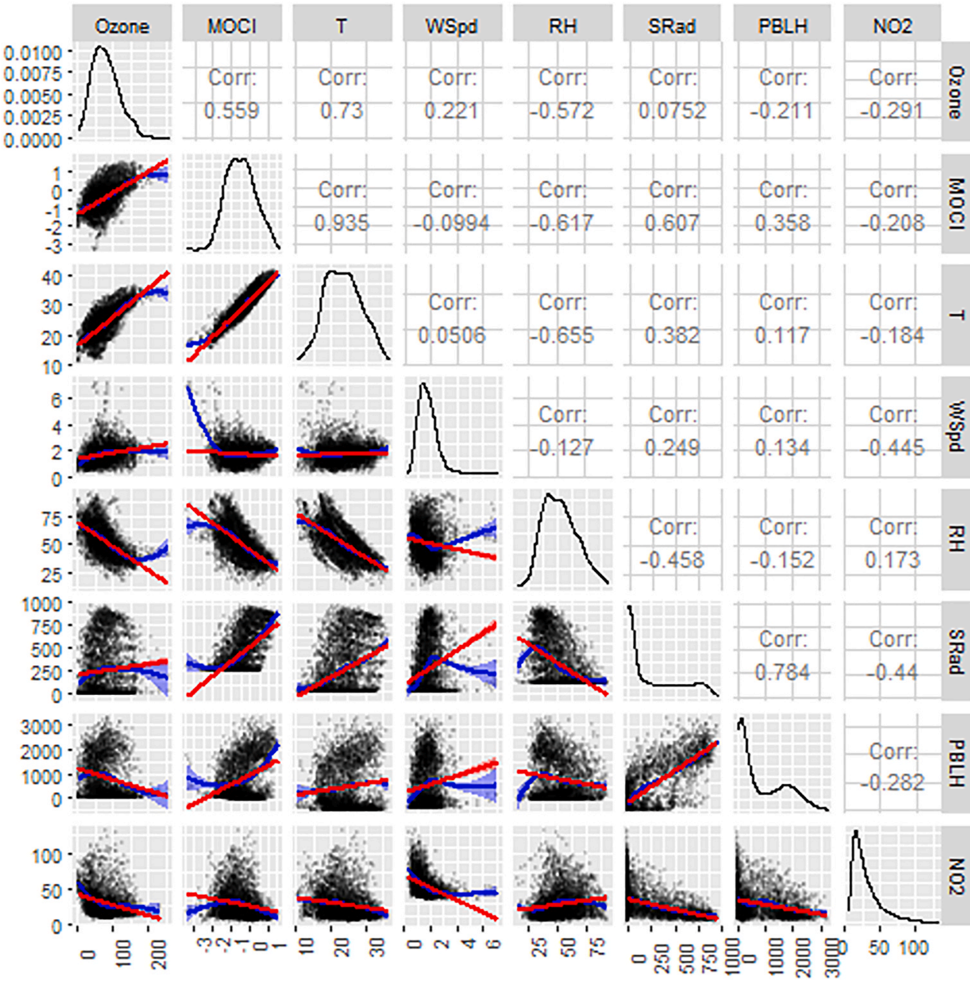

Fig. 8. Scatter plots, distribution, and correlation coefficients among all the hourly values in the dataset. T, air temperature (°C); WSpd, wind speed (m/s); RH, Relative Humidity (%); SRad, Solar Radiation (W/m^2); PBLH, Planetary Boundary Layer Height (m); NO_2 concentration. Linear regressions (red) and local moving linear regression (blue) are also shown, with shadings denoting confidence intervals. (For interpretation of the references to color in this figure legend, the reader is referred to the Web version of this article.)

−1.5 or higher than 1.5. This implies that in 40% of the days in the period May–September 2015, the outdoor thermal discomfort threshold (equal to 0.5) was exceeded. As regards the temporal distribution of the values included in the ranges considered, in May there are no exceedances of the outdoor thermal stress threshold and that in 80% of days the maximum daily MOCI is between −0.5 and 0.5 (Fig. 9b). On the contrary, in July in more than 80% of days there are conditions of outdoor thermal discomfort. In the months of June and August 45% and 60% of the days are characterized by exceeding the outdoor discomfort threshold, while in September only one day has the maximum daily MOCI greater than 0.5.

Fig. 9c shows that the daily ozone values are distributed almost equally below and above long-term objective (55% are lower than 120 μgm^{-3} and 45% are equal to or greater than 120 μgm^{-3}). In particular, the interval between 60 μgm^{-3} and 120 μgm^{-3} represents the highest percentage (equal to 49%) of the entire period, values higher than the information threshold (180 μgm^{-3}) represent 4% of the total, while the alarm threshold of 240 μgm^{-3} is exceeded only once.

Fig. 10a and b shows a good agreement between the seasonal trend of daily MOCI and daily ozone values and the scatter plot in Fig. 10c shows a strong correlation between the two quantities ($R^2 = 0.6$). As already observed in (Falasca et al., 2019), despite the presence of a significant heat wave in July 2015, the maximum daily MOCI is approximately equal to 1.5 during the ozone season, which corresponds to a surface ozone concentration of approximately 234 μgm^{-3}, the second highest value of the 2015 season. The minimum MOCI value is approximately −1.6 and the corresponding ozone concentration is approximately 87 μgm^{-3}, well below the long-term objective for human health.

3.4. Characterization of outdoor thermo-hygrometric stress events

As specified in section 2.3, in the present study outdoor thermal stress events are identified similarly to the definition of a Warm or Cold Spell Index defined by the Expert Team on Climate Change Detection Indices (ETCCDI, 2020), We define an "event" a period of at least six consecutive days characterized by maximum daily values of MOCI or ozone always above a given threshold. We set this threshold as 0.5 for MOCI and 120 μgm^{-3} for ozone. In this way, five outdoor thermal stress (MOCI) and five pollution (ozone) events have been recognized in the 2015 ozone season, with different duration and range of observations. The characteristics of the thermal stress events (start and end dates, duration, extremes of the range of values observed) are reported in Table 4. The five ozone events are very similar to those identified on the basis of MOCI threshold (not shown).

Consistently with Figs. 6 and 9, Table 4 shows that July is the month most afflicted by outdoor thermal stress, both in terms of number and duration of events. In fact, two events occur in July, lasting 13 and 15 days respectively. June, like August, presents an 8 days-long event at the beginning and an event at the end. As mentioned in section 3.3 in the comment to Fig. 9, the only occurrence of a daily maximum MOCI higher than 0.5 occurs in September, and such day is part of the last event of the season.

To analyze the relationship between daily ozone and MOCI during the five thermal stress events, Fig. 11 and Fig. 12 display the temporal trends of the two quantities and the boxplot of MOCI and ozone during the events and non-event periods. Fig. 11 visualizes MOCI values on the left y-axis, while it visualizes ozone concentration on the right y-axis, for

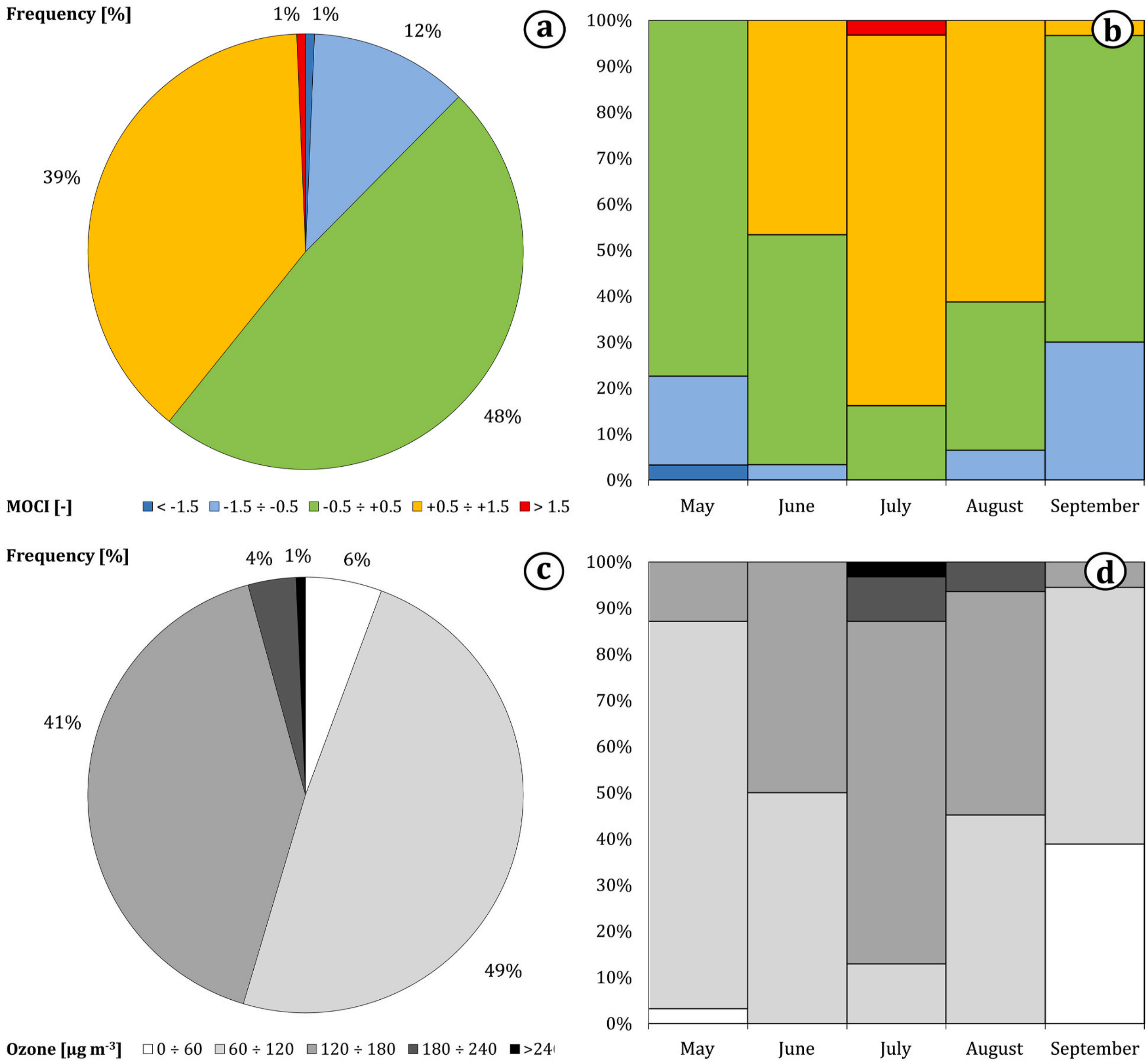

Fig. 9. Percentage distribution of the daily maximum values of MOCI and ozone in the period May–September (a–c) and in the individual months (b–d).

each thermal stress event. This figure confirms a very similar trend of daily values of MOCI and ozone, as already observed for the entire dataset of daily values (Fig. 10).

In Fig. 12 the distribution of ozone during each of the five MOCI events is compared to the distribution during non-events, and the same for MOCI distribution as a function of ozone events. In this kind of representation, the notch displays a confidence interval around the median. The event/non-event periods are clearly separated: both ozone and MOCI during events are much higher than during non-events, with high statistical significance (as denoted by the non-overlapping notches of the boxplots), while among the events the differences are statistically insignificant (as denoted by the overlapping notches).

3.4.1. The degree of correspondence between MOCI events and ozone events

In Table 5 we further quantify the degree of correspondence between MOCI and ozone events through the 2x2 contingency table calculated with counts of event/non-event days in the two event classifications. More in detail, Table 5 is based on MOCI computed using the variables both recorded by the OMD weather station (hereinafter, recorded MOCI) and simulated by the WRF model (hereinafter, simulated MOCI). In this table, a, b, c and d represent the number of hits, false alarms, misses and correct negatives respectively. Based on these outcomes, the Hit Rate (HR) and the False Alarm Rate (FR) can be computed. The HR and FR are defined as (equations (8) and (9)):

$$HR = \frac{a}{a + c} \tag{8b}$$

and

$$FR = \frac{b}{b + d} \tag{9}$$

Both parameters have a range from 0 to 1. In this application, the HR represents a measure of the probability of detection of ozone events thanks to the MOCI events, while the FR represents a measure of the probability of false detection of ozone events by means of MOCI events.

The overestimation of the MOCI values by the WRF model leads to an increase in the values of a and c (sum of the number of days of MOCI events) and a decrease in the values of c and d (sum of the days of non-event days of MOCI). However, the sum of a and c and b and d is the same in Table 5, as it represents the sum of the days of ozone events and non-ozone events, respectively. Therefore, using the simulated MOCI entails an increase in the days of ozone events detected by MOCI events (53 instead of 48, Table 5) and a decrease in the days of ozone events not

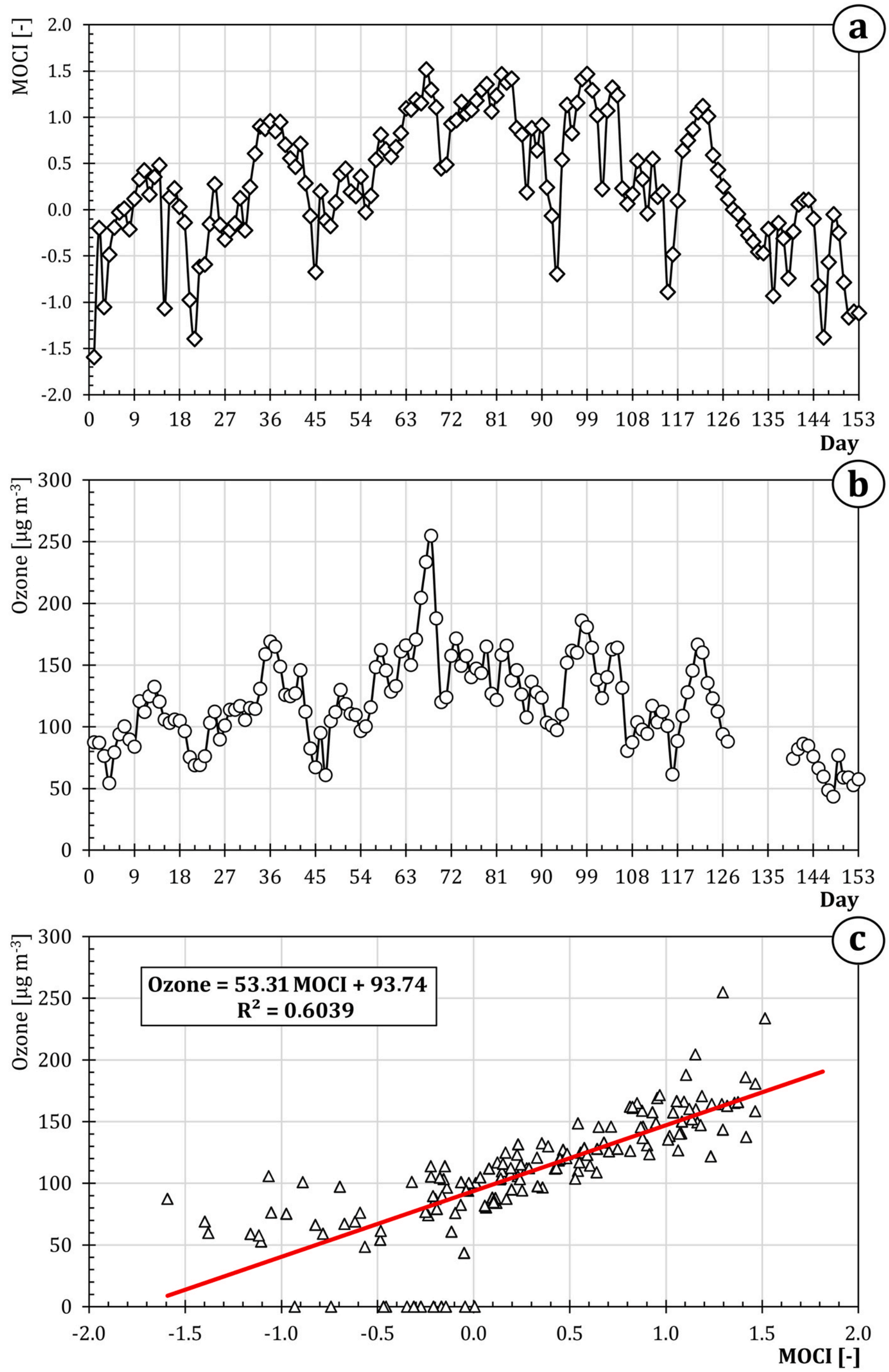

Fig. 10. Daily maximum data for MOCI and ozone: a) seasonal trends; b) scatter plot with correlation coefficient.

detected by MOCI events (3 instead of 8, Table 5). On the other side, the model's overestimation of the MOCI involves 9 days of false alarms procured by simulated MOCI rather than 3 days of false alarms procured by recorded MOCI (Table 5).

The HR is equal to 0.86 for the recorded MOCI, while it is equal to 0.95 for the simulated MOCI. The FR is equal to 0.03 and 0.09 for the recorded and simulated MOCI, respectively. Using the simulated MOCI instead of the recorded MOCI, both HR and FR increase. In particular, HR reaches almost the ideal value characteristic of a perfect correspondence, i.e. 1. On the other side, although generally speaking the increase of FR implies a decay of the MOCI events-ozone events correspondence, in this application such increase appears to be defensive and not damaging to public health.

4. Discussion

The analysis performed in this study allows to correlate MOCI values with ozone concentrations during the May–September period of the year 2015 and to achieve the following findings:

– there is a time phase shift between the maximum values in the daily cycles of MOCI (mean of the hourly measured values) and ozone (8 h running mean of the hourly measured values), with a delay of about 5 h of the ozone maximum compared to MOCI. This means that, although the perception of thermal stress occurs in the central hours of the day, even the early hours of the evening is unsafe in terms of ozone concentration.

Table 4
Characteristics of the outdoor thermal stress events: start and end dates, duration (days), extremes of the range of values observed for MOCI and ozone.

Event	Start – End Dates	Duration (days)	[a]Minimum daily MOCI during the event	[b]Maximum daily MOCI during the event	[a]Minimum daily O38h during the event	[b]Maximum daily O38h during the event
1	2nd Jun – 9th Jun	8	0.5	0.9	114.5	169.1
2	26th Jun – 8th Jul	13	0.5	1.5	128.4	254.8
3	11th Jul – 25th Jul	15	0.8	1.5	121.7	171.5
4	2nd Aug – 9th Aug	8	0.5	1.5	110.1	185.9
5	26th Aug – 1st Sep	7	0.6	1.1	108.8	166.6

[a] Minimum among daily values of the parameter for each event.
[b] Maximum among daily values of the parameter for each event.

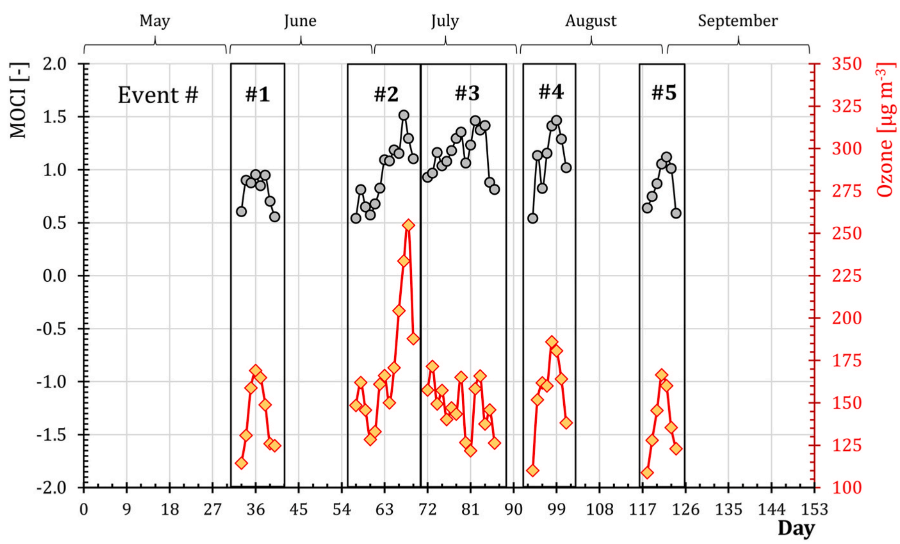

Fig. 11. Temporal trends of daily MOCI and O_3 during the thermal stress events.

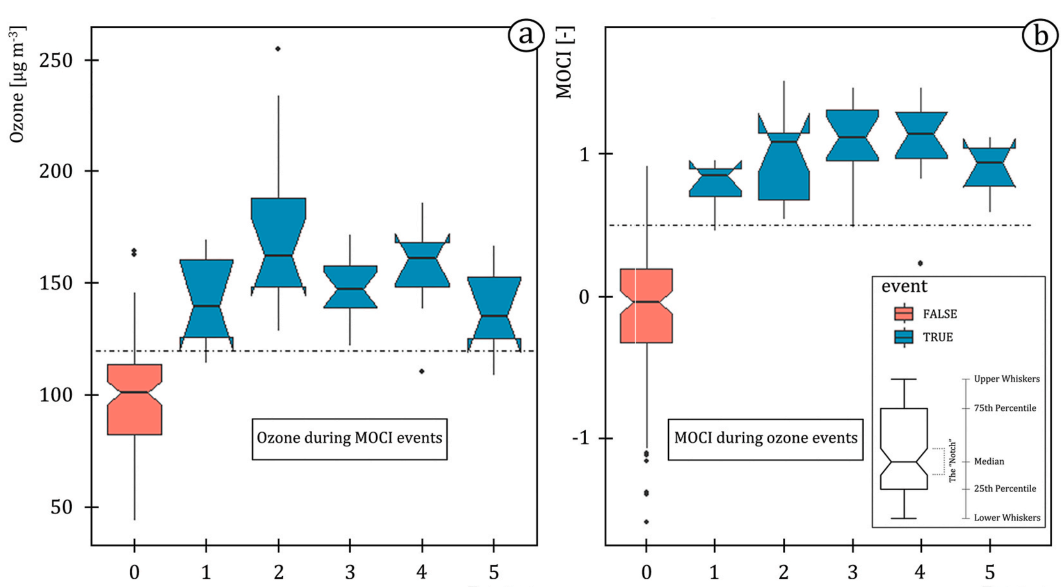

Fig. 12. Boxplot of (a) O_3 during MOCI events (6+ consecutive days > 0.5) and of (b) MOCI during O_3 events (6+ consecutive days > 120 μgm^{-3}). The notch in each boxplot denotes the confidence interval.

Table 5
Contingency table of the correspondence of recorded and simulated MOCI and ozone events (days).

MOCI events		Ozone events	
		Event	Non-Event
Recorded	Event	a = 48	b = 3
	Non-event	c = 8	d = 94
Simulated	Event	a = 53	b = 9
	Non-event	c = 3	d = 88

- Based on the high correlation factor, MOCI proves to be an ozone enhancement factor in the same way as temperature, enclosing the effects of the weather quantities composing it.
- All thermal stress events (daily MOCI $\geq$ 0.5) are characterized by values of the daily ozone higher than 100 μgm^{-3}, guideline level specified by the World Health Organization. Even if most of such values do not represent exceedances of the long-term objective (equal to 120 μgm^{-3}) defined in the effective European Directive on Air Quality, they constitute a risk for the health of people.
- The strong correlation between daily MOCI and ozone during the thermal stress events implies that as the MOCI (and therefore thermal discomfort) increases, the daily ozone concentration increases consequently. Therefore, in these periods there is a double risk for the population, both in terms of outdoor discomfort and in terms of air quality.
- The classification of recorded MOCI events appears to be a good predictor of ozone event classification with a hit rate of 0.86, indicating that 86% of days during ozone events are correctly predicted by MOCI events, and a low false alarm rate of 3%.
- The use of the MOCI simulated by the WRF model improves the hit rate getting it up to 95% and at the same time increases the false alarm rate from 3% to 9%.

5. Conclusions

In the present article an investigation of the May–September period (defined as the "ozone season") of 2015 has been performed in terms of the outdoor thermo-hygrometric comfort index MOCI and ground levels of ozone in Milan (Northern Italy). This city was chosen as a case study because it is a large urban area, heavily populated, located in the center of the Po Valley, characterized by critical air quality issues.

The main findings of this study concern the strong correlation between the daily MOCI and daily levels of surface ozone, both during the whole ozone season (correlation coefficient equal to 0.6) and during the individual thermal discomfort events (correlation coefficients between ~0.6 and ~0.8). Moreover, results show that thermo-hygrometric stress conditions generally add on poor air quality conditions, with significant implications on the human well-being and health, especially for subjects at risk (e.g. chronic ill and elderly).

The evidence of co-existence of thermo-hygrometric discomfort and poor air quality circumstances can also have implications from the point of view of forecasting and control methods of high levels of surface ozone. In fact, given the reliability achieved by the forecast weather models, the knowledge of the correlation between the two quantities can be useful for making a prediction of associated events of MOCI and high concentrations of surface ozone. Furthermore, since it is not always possible to have records on ground level ozone, it would be useful to determine statistically robust correlations that can help predict these concentrations as a function of easy-to-monitor environmental indicators (using data from local meteorological variables, such as for MOCI).

Air quality models are a valuable tool for predicting high concentrations of ground level ozone. Such models are quite complex and require input data that have to be accurate to ensure good performance. In the past we studied some aspects of this subject (e.g. (Falasca and Curci, 2018b)).

In the present study, results show that severe ozone events and MOCI can be predicted by means of weather variables, without the use of chemical modules, for example with the WRF model. This tool could not replace air quality models in quantifying ozone concentrations, but it could provide information for the identification of critical conditions for the public health. Furthermore, the use of the WRF model (or similar models) allows to detect severe ozone events both spatially and temporally.

Although the strong correlation identified is highly specific to the site considered and this study relates to a single pair of weather-air quality stations, this study may constitute the first step in the exploration of a research field of which little is known at present, and motivates the possible development of a new joint thermal stress-air pollution index.

Author contribution

Serena Falasca, Conceptualization, Methodology, Investigation, Software, Validation, Writing - original draft. Gabriele Curci, Investigation, Software, Visualization, Writing - review & editing. Ferdinando Salata, Conceptualization, Methodology, Visualization, Data curation, Writing - review & editing, Supervision

Declaration of competing interest

The authors declare that they have no known competing financial interests or personal relationships that could have appeared to influence the work reported in this paper.

Acknowledgements

The computational resources for WRF runs were provided by Laboratori Nazionali del Gran Sasso (LNGS) and CINECA. We acknowledge the CINECA award under the ISCRA initiative, for the availability of high-performance computing resources and support. We also acknowledge Osservatorio Milano Duomo (OMD) Foundation for providing observations of the ClimateNetwork® stations and ARPA Lombardia for providing concentrations of surface ozone.

References

ARPA - Environmental issues/Air/Detection network, 2020. ARPA Lomb. - Reg. Environ. Prot. Agency Lomb. https://www.arpalombardia.it/Pages/Aria/Rete-di-rilevamento.aspx. accessed 5.5.20.

Axiak, V., Sammut, A., 2002. The coast and freshwater resources. State Environ. Rep. Malta 349–414, 2002.

Block, M.L., Elder, A., Auten, R.L., Bilbo, S.D., Chen, H., Chen, J.C., Cory-Slechta, D.A., Costa, D., Diaz-Sanchez, D., Dorman, D.C., Gold, D.R., Gray, K., Jeng, H.A., Kaufman, J.D., Kleinman, M.T., Kirshner, A., Lawler, C., Miller, D.S., Nadadur, S.S., Ritz, B., Semmens, E.O., Tonelli, L.H., Veronesi, B., Wright, R.O., Wright, R.J., 2012. The outdoor air pollution and brain health workshop. Neurotoxicology 33, 972–984. https://doi.org/10.1016/j.neuro.2012.08.014.

Chang, J.C., Hanna, S.R., 2004. Air quality model performance evaluation. Meteorol. Atmos. Phys. 87, 167–196. https://doi.org/10.1007/s00703-003-0070-7.

Chang, K.L., Petropavlovskikh, I., Cooper, O.R., Schultz, M.G., Wang, T., 2017. Regional trend analysis of surface ozone observations from monitoring networks in eastern North America, Europe and East Asia. Elementa 5, 1–22. https://doi.org/10.1525/elementa.243.

Ciancio, V., Falasca, S., Golasi, I., Curci, G., Coppi, M., Salata, F., 2018. Influence of input climatic data on simulations of annual energy needs of a building: EnergyPlus and WRF modeling for a case study in Rome (Italy). Energies 11, 2835. https://doi.org/10.3390/en11102835.

Deng, J.Y., Wong, N.H., 2020. Impact of urban canyon geometries on outdoor thermal comfort in central business districts. Sustain. Cities Soc. 53, 101966. https://doi.org/10.1016/j.scs.2019.101966.

EEA, 2016. 2. Tropospheric Ozone: Background Information.

ETCCDI, 2020. Climate Change Indices - Definitions of the 27 Core Indices [WWW Document]. http://etccdi.pacificclimate.org/list_27_indices.shtml. accessed 6.2.20.

European Environment Agency, 2017. Air Quality in Europe — 2017. EEA Technical Report. https://doi.org/10.2800/850018.

European Environmental Agency, 2019. Air Quality in Europe — 2019 Report — EEA Report No 10/2019. https://doi.org/10.2800/822355.

Falasca, S., Catalano, F., Moroni, M., 2016. Numerical study of the daytime planetary boundary layer over an idealized urban area: influence of surface Properties, anthropogenic heat flux, and geostrophic wind intensity. J. Appl. Meteorol. Climatol. 55, 1021–1039. https://doi.org/10.1175/JAMC-D-15-0135.1.

Falasca, S., Ciancio, V., Salata, F., Golasi, I., Rosso, F., Curci, G., 2019. High albedo materials to counteract heat waves in cities: an assessment of meteorology, buildings energy needs and pedestrian thermal comfort. Build. Environ. 163, 106242. https://doi.org/10.1016/j.buildenv.2019.106242.

Falasca, S., Curci, G., 2018a. Impact of highly reflective materials on meteorology, PM10 and ozone in urban areas: a modeling study with WRF-CHIMERE at high resolution over milan (Italy). Urban Sci 2, 18. https://doi.org/10.3390/urbansci2010018.

Falasca, S., Curci, G., 2018b. High-resolution air quality modeling: sensitivity tests to horizontal resolution and urban canopy with WRF-CHIMERE. Atmos. Environ. 187, 241–254. https://doi.org/10.1016/j.atmosenv.2018.05.048.

Gilliland, F.D., 2009. Outdoor air pollution, genetic susceptibility, and asthma management: opportunities for intervention to reduce the burden of asthma. Pediatrics 123, 14–16. https://doi.org/10.1542/peds.2008-2233G.

Golasi, I., Salata, F., de Lieto Vollaro, E., Coppi, M., de Lieto Vollaro, A., 2016. Thermal perception in the mediterranean area: comparing the mediterranean outdoor comfort index (MOCI) to other outdoor thermal comfort indices. Energies 9, 1–16. https://doi.org/10.3390/en9070550.

Hanna, S., Chang, J., 2012. Acceptance criteria for urban dispersion model evaluation. Meteorol. Atmos. Phys. 116, 133–146. https://doi.org/10.1007/s00703-011-0177-1.

Jacob, D.J., Winner, D.A., 2009. Effect of climate change on air quality. Atmos. Environ. 43, 51–63. https://doi.org/10.1016/j.atmosenv.2008.09.051.

Jenkin, M.E., Clemitshaw, K.C., 2002. Chapter 11 Ozone and other secondary photochemical pollutants: chemical processes governing their formation in the planetary boundary layer. Dev. Environ. Sci. 1, 285–338. https://doi.org/10.1016/S1474-8177(02)80014-6.

Krug, A., Fenner, D., Holtmann, A., Scherer, D., 2019. Occurrence and coupling of heat and ozone events and their relation to mortality rates in Berlin, Germany, between 2000 and 2014. Atmosphere 10. https://doi.org/10.3390/atmos10060348.

Krüger, E.L., Minella, F.O., Rasia, F., 2011. Impact of urban geometry on outdoor thermal comfort and air quality from field measurements in Curitiba. Brazil. Build. Environ. 46, 621–634. https://doi.org/10.1016/j.buildenv.2010.09.006.

Lee, K., Parkhurst, W.J., Xue, J., Özkaynak, A.H., Neuberg, D., Spengler, J.D., 2004. Outdoor/indoor/personal ozone exposures of children in nashville, Tennessee. J. Air Waste Manag. Assoc. 54, 352–359. https://doi.org/10.1080/10473289.2004.10470904.

Martilli, A., Clappier, A., Rotach, M.W., 2002. MESOSCALE MODELS 261–304.

Meehl, G.A., Tebaldi, C., Tilmes, S., Lamarque, J.F., Bates, S., Pendergrass, A., Lombardozzi, D., 2018. Future heat waves and surface ozone. Environ. Res. Lett. 13 https://doi.org/10.1088/1748-9326/aabcdc.

Municipality of Milan, 2020. Municipality of Milan - Resident Population [WWW Document]. https://www.comune.milano.it/aree-tematiche/dati-statistici/pubblicazioni/popolazione-residente-a-milano. accessed 5.25.20.

National Centers for Environmental Prediction/National Weather Service/NOAA/U.S, 2000. NCEP FNL Operational Model Global Tropospheric Analyses, Continuing from July 1999. Research Data Archive at the National Center for Atmospheric Research, Computational and Information Systems Laboratory. https://doi.org/10.5065/D6M043C6.

Orru, H., Åström, C., Andersson, C., Tamm, T., Ebi, K.L., Forsberg, B., 2019. Ozone and heat-related mortality in Europe in 2050 significantly affected by changes in climate, population and greenhouse gas emission. Environ. Res. Lett. 14, 74013. https://doi.org/10.1088/1748-9326/ab1cd9.

Otero, N., Sillmann, J., Schnell, J.L., Rust, H.W., Butler, T., 2016. Synoptic and meteorological drivers of extreme ozone concentrations over Europe. Environ. Res. Lett. 11, 24005. https://doi.org/10.1088/1748-9326/11/2/024005.

Parliament, T.H.E.E., Council, T.H.E., The, O.F., Union, P., 2008. 11.6.2008.

Pollock, J., Shi, L., Gimbel, R.W., 2017. Outdoor environment and pediatric asthma: an update on the evidence from North America. Canc. Res. J. https://doi.org/10.1155/2017/8921917, 2017.

Porter, W.C., Heald, C.L., 2019. The mechanisms and meteorological drivers of the summertime ozoneerature relationship. Atmos. Chem. Phys. 19, 13367–13381. https://doi.org/10.5194/acp-19-13367-2019.

Porter, W.C., Heald, C.L., Cooley, D., Russell, B., 2015. Investigating the observed sensitivities of air-quality extremes to meteorological drivers via quantile regression. Atmos. Chem. Phys. 15, 10349–10366. https://doi.org/10.5194/acp-15-10349-2015.

Presidente, I.L., Repubblica, D., 2010. Attuazione della direttiva 2008/50/CE relativa alla qualità dell â€™ aria ambiente e per un â€™ aria più pulita in Europa. 1.

Pyrgou, A., Hadjinicolaou, P., Santamouris, M., 2018. Enhanced near-surface ozone under heatwave conditions in a Mediterranean island. Sci. Rep. 8, 1–10. https://doi.org/10.1038/s41598-018-27590-z.

Rosso, F., Golasi, I., Castaldo, V.L., Piselli, C., Pisello, A.L., Salata, F., Ferrero, M., Cotana, F., de Lieto Vollaro, A., 2018. On the impact of innovative materials on outdoor thermal comfort of pedestrians in historical urban canyons. Renew. Energy 118, 825–839. https://doi.org/10.1016/j.renene.2017.11.074.

Salata, F., Golasi, I., Ciancio, V., Rosso, F., 2018a. Dressed for the season: clothing and outdoor thermal comfort in the Mediterranean population. Build. Environ. 146, 50–63. https://doi.org/10.1016/j.buildenv.2018.09.041.

Salata, F., Golasi, I., de Lieto Vollaro, R., de Lieto Vollaro, A., 2016a. Outdoor thermal comfort in the Mediterranean area. A transversal study in Rome, Italy. Build. Environ. 96, 46–61. https://doi.org/10.1016/j.buildenv.2015.11.023.

Salata, F., Golasi, I., de Lieto Vollaro, R., de Lieto Vollaro, A., 2016b. Outdoor thermal comfort in the Mediterranean area. A transversal study in Rome, Italy. Build. Environ. 96, 46–61. https://doi.org/10.1016/j.buildenv.2015.11.023.

Salata, F., Golasi, I., Petitti, D., de Lieto Vollaro, E., Coppi, M., de Lieto Vollaro, A., 2017a. Relating microclimate, human thermal comfort and health during heat waves: an analysis of heat island mitigation strategies through a case study in an urban outdoor environment. Sustain. Cities Soc. 30, 79–96. https://doi.org/10.1016/j.scs.2017.01.006.

Salata, F., Golasi, I., Proietti, R., de Lieto Vollaro, A., 2017b. Implications of climate and outdoor thermal comfort on tourism: the case of Italy. Int. J. Biometeorol. https://doi.org/10.1007/s00484-017-1430-1.

Salata, F., Golasi, I., Treiani, N., Plos, R., de Lieto Vollaro, A., 2018b. On the outdoor thermal perception and comfort of a Mediterranean subject across other Koppen-Geiger's climate zones. Environ. Res. 167, 115–128. https://doi.org/10.1016/j.envres.2018.07.011.

Schultz, M.G., Schröder, S., Lyapina, O., Cooper, O.R., Galbally, I., Petropavlovskikh, I., von Schneidemesser, E., Tanimoto, H., Elshorbany, Y., Naja, M., Seguel, R.J., Dauert, U., Eckhardt, P., Feigenspan, S., Fiebig, M., Hjellbrekke, A.-G., Hong, Y.-D., Kjeld, P.C., Koide, H., Lear, G., Tarasick, D., Ueno, M., Wallasch, M., Baumgardner, D., Chuang, M.-T., Gillett, R., Lee, M., Molloy, S., Moolla, R., Wang, T., Sharps, K., Adame, J.A., Ancellet, G., Apadula, F., Artaxo, P., Barlasina, M. E., Bogucka, M., Bonasoni, P., Chang, L., Colomb, A., Cuevas-Agulló, E., Cupeiro, M., Degorska, A., Ding, A., Fröhlich, M., Frolova, M., Gadhavi, H., Gheusi, F., Gilge, S., Gonzalez, M.Y., Gros, V., Hamad, S.H., Helmig, D., Henriques, D., Hermansen, O., Holla, R., Hueber, J., Im, U., Jaffe, D.A., Komala, N., Kubistin, D., Lam, K.-S., Laurila, T., Lee, H., Levy, I., Mazzoleni, C., Mazzoleni, L.R., McClure-Begley, A., Mohamad, M., Murovec, M., Navarro-Comas, M., Nicodim, F., Parrish, D., Read, K. A., Reid, N., Ries, L., Saxena, P., Schwab, J.J., Scorgie, Y., Senik, I., Simmonds, P., Sinha, V., Skorokhod, A.I., Spain, G., Spangl, W., Spoor, R., Springston, S.R., Steer, K., Steinbacher, M., Suharguniyawan, E., Torre, P., Trickl, T., Weili, L., Weller, R., Xu, X., Xue, L., Zhiqiang, M., 2017. Tropospheric Ozone Assessment Report, Links to Global Surface Ozone Datasets. Suppl. to Schultz, MG al. Tropospheric Ozone Assess. Rep. Database Metrics Data Glob. Surf. Ozone Obs. Elem. - Sci. Anthr. 558, p. 26. https://doi.org/10.1594/PANGAEA.876108, 10.1525/elementa.244.

Skamarock, W.C., Klemp, J.B., Dudhi, J., Gill, D.O., Barker, D.M., Duda, M.G., Huang, X.-Y., Wang, W., Powers, J.G., 2008. A description of the advanced research WRF version 3. Natl. Cent. Atmos. Res. Boulder, CO, USA 113. https://doi.org/10.5065/D6DZ069T.

Stowell, JD, Kim, Y, Gao, Y, Fu, JS, Chang, HH, Liu, Y, 2017. The impact of climate change and emissions control on future ozone levels: Implications for human health. Environ Int 108, 41–50. https://doi.org/10.1016/J.ENVINT.2017.08.001.

Von Mutius, E., 2000. The environmental predictors of allergic disease. J. Allergy Clin. Immunol. 105, 9–19. https://doi.org/10.1016/S0091-6749(00)90171-4.

Wilhelm, M., Qian, L., Ritz, B., 2009. Outdoor air pollution, family and neighborhood environment, and asthma in LA FANS children. Health Place 15, 25–36. https://doi.org/10.1016/j.healthplace.2008.02.002.

World Health Organization, W., 2005. WHO Air Quality Guidelines for Particulate Matter, Ozone, Nitrogen Dioxide and Sulfur Dioxide: Global Update 2005, pp. 1–21. https://doi.org/10.1016/0004-6981(88)90109-6.

Yuan, C., Ng, E., Norford, L.K., 2014. Improving air quality in high-density cities by understanding the relationship between air pollutant dispersion and urban morphologies. Build. Environ. 71, 245–258. https://doi.org/10.1016/j.buildenv.2013.10.008.